Extension of high-order harmonic cutoff frequency by synthesizing the waveform of a laser field via the optimization of classical electron trajectory in the laser field*

Zhao Di(赵 迪)† and Li Fu-Li(李福利)

Department of Applied Physics, Xi'an Jiaotong University, Xi'an 710049, *China*

(Received 17 December 2012; revised manuscript received 30 January 2013)

We theoretically investigate high-order harmonic generation by employing strong-field approximation (SFA) and present a new approach to the extension of the high-order harmonic cutoff frequency via an exploration of the dependence of high-order harmonic generation on the waveform of laser fields. The dependence is investigated via detailed analysis of the classical trajectories of the ionized electron moving in the continuum in the velocity–position plane. The classical trajectory consists of three sections (Acceleration Away, Deceleration Away, and Acceleration Back), and their relationship with the electron recollision energy is investigated. The analysis of classical trajectories indicates that, besides the final (Acceleration Back) section, the electron recollision energy also relies on the previous two sections. We simultaneously optimize the waveform in all three sections to increase the electron recollision energy, and an extension of the cutoff frequency up to $I_p + 20.26U_p$ is presented with a theoretically synthesized waveform of the laser field.

Keywords: high-order harmonic generation, classical electron trajectory, cutoff frequency extension

PACS: 42.65.Ky, 32.80.Wz **DOI:** 10.1088/1674-1056/22/6/064215

1. Introduction

Coherent light sources in the vacuum ultraviolet and X-ray regions provide an ideal tool for probing living biological structures and controlling the dynamics of atomic systems. For example, an intense ultrafast water window (between K absorption edges of carbon and oxygen 284 eV–545 eV) X-ray pulse would allow us to capture an image of live cells by instantaneously halting their motion, and preserving their native structural details without any information loss introduced in the sample's preparation process for electron microscopy.[1–3] On the other hand, study of the inner-shell and core electronic transition processes requires the probing photon frequency to be in the vacuum ultraviolet and X-ray regions. In the past two decades, high-order harmonic generation (HHG) by intense laser–atom interactions has been proposed as an ideal method to realize coherent ultrashort light sources in the vacuum ultraviolet and X-ray regions on a so-called table-top systems as opposed to large free-electron-laser facilities.[4–7]

The harmonic spectrum of HHG shows the general feature that: the intensity decreases at low harmonic frequencies, exhibits a plateau over a broadband frequency range, and then abruptly drops at the so-called cutoff frequency. For a monochromatic laser field, the cutoff frequency (energy) can approximately be written as $E_{\rm cutoff} = \hbar\omega_{\rm cutoff} = I_p + 3.17U_p$,[8] where I_p and $U_p = \mathcal{E}^2/(4\omega^2)$ ($\mathcal{E}$ is the field amplitude) are the ionization potential of the electron and the ponderomotive potential of the laser field, respectively. From this result one can see that there are two possible ways to extend the cutoff frequency to the X-ray regions: increasing the field amplitude $\mathcal{E}$, and applying the driving fields with a longer wavelength. However, increasing the field amplitude leads to higher free-electron density in the interaction volume, which will depress the generation efficiency of harmonics.[9–11] On the other hand, the field with longer wavelength results in the reduction of harmonic yield,[12,13] due to increasing trajectory duration.[14] Mixing of different color laser fields is one of the schemes that are suggested to overcome these limitations.[15] Many schemes have been proposed, for example, subharmonic and harmonic fields,[16–25] chirped pulses,[26–29] and static fields.[30–35] Moreover, molecules as a target medium are also employed to extend the cutoff frequency.[36–38]

Treating the electron in continuum classically within the strong-field approximation,[39–41] one can divide the electron trajectories into three sections:[8,14] (i) "Acceleration Away" from the parent ion after ionization; (ii) "Deceleration Away" after the field changes sign; (iii) "Acceleration Back" to the parent ion till the recombination happens, converting its kinetic energy plus potential energy into the harmonic radiation. Thus the cutoff frequency in the harmonic spectrum is equal to the sum of the electron's ionization potential and the maximum kinetic energy at the time of recombination, i.e., $E_{\rm cutoff} = I_p + E_{\rm max}$, where $E_{\rm max}$ is the maximum kinetic (recol-

*Project supported by the National Basic Research Program of China (Grant No. 2010CB923102), the Special Prophase Project on the National Basic Research Program of China (Grant No. 2011CB311807), and the National Natural Science Foundation of China (Grant No. 11074199).

†Corresponding author. E-mail: zhaodifrog@gmail.com

© 2013 Chinese Physical Society and IOP Publishing Ltd

lision) energy that the electron gains from the laser field in the continuum, and depends on the classical motion in the laser field before the electron recombines with its parent ion. It is suggested that optimizing the waveform of a laser field is an accessible way to extend the cutoff frequency without increasing the field amplitude.

Recently, Chipperfield *et al.*[14] proposed an optimized waveform and increased the cutoff frequency by a factor of 2.5 while maintaining the harmonic yield. Their approach was under the assumption that the electron oscillation period in the continuum and the average power of the field over that period were fixed. Moreover, Pérez-Hernández *et al.*[14] suggested a waveform consisting of two delayed pulses and raised the cutoff frequency up to $I_p + 5.5U_p$ by optimizing the delay time. Their analysis showed that the underlying physics responsible for the extension was the shaping of the laser field where the two-component pulses overlapped. However, both works focused mainly on the role of the waveform in the final (Acceleration Back) section of the classical electron trajectories, and little attention was paid to the other sections of trajectories. In this paper, we study the HHG process by employing the strong-field approximation and investigate the dependence of the electron recollision energy on the waveform of laser fields in different sections of the classical electron trajectory via a detailed analysis of the classical electron trajectories in the velocity–position plane. Our study shows that not only the waveform in the final section of the trajectory is important for the determination of the electron recollision energy, but also the waveform in the other two sections have large impacts on the electron recollision energy. In this paper, all three sections are simultaneously optimized, and an extension of the cutoff frequency up to $I_p + 20.26U_p$ is presented under a theoretically synthesized laser field waveform.

This paper is organized as follows. In Section 2. we outline the equations for the analysis of classical electron trajectories and for the calculation of harmonic spectrum within the strong-field approximation. In Section 3. we present the classical electron trajectories in the velocity–position plane and analyze the dependence of the electron recollision energy on the waveform of laser field. In Section 4, a cutoff frequency up to $I_p + 20.26U_p$ is generated after a two-step optimization of the laser field waveform, and the spectrum structure is well explained by the classical electron trajectory analysis. Finally, we summarize the analysis and results in Section 5.

2. Theoretical method

We consider a helium atom with the ionization energy $I_p = 24.59$ eV in a single-electron approximation under the influence of the intense laser field $\mathcal{E}(t)$ of linear polarization in the x direction (in the whole paper, we take the atomic units $e = m = \hbar = 1$, but express all energies in terms of eV). The Schrödinger equation for the single electron takes the form

$$\mathrm{i}\frac{\partial}{\partial t}|\Psi(\boldsymbol{x},t)\rangle = \Big[-\frac{1}{2}\nabla^2 + V(\boldsymbol{x}) - \mathcal{E}(t)x\Big]|\Psi(\boldsymbol{x},t)\rangle, \quad (1)$$

where $V(\boldsymbol{x})$ is the bounding potential of an electron around the nucleus and $\mathcal{E}(t)x$ is the dipole interaction between the electron and the laser pulse with time-dependent amplitude $\mathcal{E}(t)$. Since the laser fields we employed are in the low-frequency high-intensity regime, the time-dependent Schrödinger equation (1) can be solved analytically within the strong-field approximation.[39] Under the strong-field approximation, the time-dependent wave functions can be expanded as

$$|\Psi(t)\rangle = \mathrm{e}^{\mathrm{i}I_p t}\Big(a(t)|0\rangle + \int \mathrm{d}^3\boldsymbol{v}\, b(\boldsymbol{v},t)|\boldsymbol{v}\rangle\Big), \quad (2)$$

where $|0\rangle$ is the ground state, $a(t) \simeq 1$ is the ground-state amplitude, $|\boldsymbol{v}\rangle$ are the continuum states denoted by the kinetic momentum of the outgoing electron, and $b(\boldsymbol{v},t)$ are the amplitudes of the corresponding continuum states. Then the Schrödinger equation for $b(\boldsymbol{v},t)$ reads as

$$\dot{b}(\boldsymbol{v},t) = -\mathrm{i}\Big(\frac{\boldsymbol{v}^2}{2} + I_p\Big)b(\boldsymbol{v},t) - \mathcal{E}(t)\frac{\partial b(\boldsymbol{v},t)}{\partial v_x} + \mathrm{i}\mathcal{E}(t)d_x(\boldsymbol{v}), \quad (3)$$

where $\boldsymbol{d}(\boldsymbol{v}) = \langle \boldsymbol{v}|\boldsymbol{x}|\boldsymbol{0}\rangle$ denotes the atomic dipole matrix element for the bound-free transition and $d_x(\boldsymbol{v})$ is the component parallel to the polarization axis. When writing Eq. (3), the depletion of the ground state is neglected by setting $a(t) = 1$ on the right-hand side. By solving Eq. (3), we obtain the expression for the amplitude $b(\boldsymbol{v},t)$

$$b(\boldsymbol{v},t) = \mathrm{i}\int_0^t \mathrm{d}t'\mathcal{E}(t')d_x(\boldsymbol{v}+\boldsymbol{A}(t)-\boldsymbol{A}(t')) \times \exp\Big\{-\mathrm{i}\int_{t'}^t \mathrm{d}t''\big[(\boldsymbol{v}+\boldsymbol{A}(t)-\boldsymbol{A}(t''))^2/2 + I_p\big]\Big\}, \quad (4)$$

where $\boldsymbol{A}(t) = -\int_{-\infty}^t \mathcal{E}(t')\mathrm{d}t'$ is the vector potential of the laser field. Considering only the transitions back to the ground state and introducing a canonical momentum $\boldsymbol{p} = \boldsymbol{v} + \boldsymbol{A}(t)$, from Eqs. (2) and (4), one can obtain the x component of the time-dependent dipole moment

$$\begin{aligned} D(t) &= \langle\Psi(t)|x|\Psi(t)\rangle \\ &= \mathrm{i}\int_0^t \mathrm{d}t' \int \mathrm{d}^3\boldsymbol{p}\mathcal{E}(t')d_x^*(\boldsymbol{p}-\boldsymbol{A}(t))\,\mathrm{e}^{-\mathrm{i}S(\boldsymbol{p},t,t')} \\ &\quad \times d_x(\boldsymbol{p}-\boldsymbol{A}(t')) + \mathrm{c.c.}, \end{aligned} \quad (5)$$

where

$$S(\boldsymbol{p},t,t') = \int_{t'}^t \mathrm{d}t''\Big(\frac{[\boldsymbol{p}-\boldsymbol{A}(t'')]^2}{2} + I_p\Big). \quad (6)$$

The spectrum of HHG is given by the product of the Fourier transform of $D(t)$ and Ω^2 (Ω is the frequency of the emitted harmonics)[42]

$$\boldsymbol{a}(\Omega) = \Omega^2\tilde{D}(\Omega), \quad (7)$$

where

$$\tilde{D}(\Omega) = \int_0^{T_p}\frac{\mathrm{d}t}{T_p}D(t)\exp(\mathrm{i}\Omega t) \quad (8)$$

and T_p is the duration of the driving field.

In Refs. [40] and [41], it has been proved that the quantum details of the ionization and recombination of an electron bounded by a nucleus and driven by a strong laser pulse can be neglected. Thus, it is reasonable to treat the motion of electron in continuum with classical mechanics. In order to analyze the classical electron trajectory of an electron, we assume that the electron is ionized from the nucleus at t_1 and recombines with the parent ion at t_2. Then its velocity $V(t)$ and position from the parent ion $S(t)$ at t $(t_1 \leq t \leq t_2)$ can be expressed as

$$V(t) = \int_{t_1}^{t} \mathcal{E}(t)\,\mathrm{d}t, \tag{9}$$

$$S(t) = \int_{t_1}^{t} \left(\int_{t_1}^{t'} \mathcal{E}(t'')\,\mathrm{d}t'' \right) \mathrm{d}t'. \tag{10}$$

Given the driving field and the ionization time t_1 of an electron, one can obtain the velocity and position of the electron during propagation in the continuum. The recombination time t_2 depends on the ionization time t_1 [20,21] and is determined by the equation

$$\int_{t_1}^{t_2} \left(\int_{t_1}^{t'} \mathcal{E}(t'')\,\mathrm{d}t'' \right) \mathrm{d}t' = 0. \tag{11}$$

Thus the recollision energy E_k of an electron depends on both the ionization time t_1 and the recombination time t_2 is

$$E_k = \frac{1}{2} \left(\int_{t_1}^{t_2} \mathcal{E}(t)\,\mathrm{d}t \right)^2. \tag{12}$$

Therefore, for a given ionization time, one can obtain a close trajectory in the $V(t)$ versus $S(t)$ plane, which has a fixed recollision energy.

With a given waveform of a laser field, the harmonic spectrum is calculated by employing Eqs. (5) and (7) within the strong-field approximation. The plateau structure and cutoff frequency in the spectrum can be related to the classical electron trajectories that propagate in the continuum. We will present a detailed study of the classical electron trajectories in the velocity–position plane by employing Eqs. (9)–(12), and show that the great enhancement of the cutoff frequency can be achieved by optimizing the waveform of the driving laser field.

3. Analysis of the classical electron trajectories

In this section, we use the same waveform of the laser pulse as in Ref. [41] and try to relate a trajectory with the largest recollision energy to the cutoff frequency of the HHG spectrum according to the analysis of trajectories in the velocity–position plane. Then we provide a proposal to modify the trajectory by changing the waveform of the laser pulses for extending the cutoff frequency.

The laser field interacting with the electron is composed of two delayed pulses and is given by

$$\mathcal{E}_1(t) = \mathcal{E}_0(t + \tau/2) + \mathcal{E}_0(t - \tau/2)\,\mathrm{e}^{\mathrm{i}\pi}, \tag{13}$$

where $\tau = 0.8T_0$ is the delay time and the laser pulse is described by

$$\mathcal{E}_0(t) = \begin{cases} F_0 \cos^2(\frac{t}{T_0}\pi)\sin(\omega t), & \text{if} \quad |t| < T_0, \\ 0, & \text{otherwise.} \end{cases} \tag{14}$$

In Eq. (14), F_0 is the peak amplitude of the laser pulse corresponding to $I = 5 \times 10^{14}$ W·cm^{-2}, $\omega = 0.057$ a.u. (a.u. is the abbreviation for atomic unit) is the central frequency corresponding to wavelength $\lambda = 800$ nm, T_0 is the optical cycle of the laser field, $\cos^2(t\pi/T_0)$ is the pulse envelope, and F_0 is used to calculate $U_p = F_0^2/(4\omega^2)$, which is taken as the reference energy unit in this paper. The electric fields of $\mathcal{E}_1(t)$ (solid line) and $\mathcal{E}_0(t)$ (dotted line) are plotted in Fig. 1(a), where the dashed line represents F_0.

The harmonic spectrum generated from the He atom by the field $\mathcal{E}_1(t)$ is presented in Fig. 1(b). The spectrum shows a plateau structure with the cutoff frequency up to 193 eV $(I_p + 5.5U_P)$. The cutoff frequency is the same as that obtained in Ref. [41]. To study the effect of the shaped waveform of the laser field, Pérez-Hernández *et al.* [41] analyzed the position $S(t)$ of the electron as a function of time and the dependence of the recollision energy on the ionization and recombination times. However, their analysis cannot provide sufficient information on the electron trajectory, especially the electron's velocity $V(t)$ during its propagation in the continuum, which is directly related to the recollision energy of the electron. Analyzing velocity $V(t)$ and position $S(t)$ of the electron together shall provide a more comprehensive understanding about the effects of the shaped waveform on the classical electron trajectories. Based on the analysis in the velocity–position plane, we can optimize the waveform of the laser field to achieve the extension of the cutoff frequency.

Given an ionization time, one can obtain the corresponding recombination time and the recollision energy E_k from Eqs. (11) and (12), respectively. Figure 1(c) presents the dependence of the recollision energy on the ionization time (black solid square) and recombination time (red open cycle). The maximum recollision energy $E_{max} = 165$ eV $(5.5U_p)$ corresponds to the cutoff trajectory [sketched with blue dotted line in Fig. 1(c)]. It is observed in Fig. 1(c) that each of the recollision energies smaller than the maximum one correspond to two ionization and recombination moments, i.e., two trajectories. The ionization and recombination times of the trajectories with the recollision energies $E_k = 50$ eV $(1.67U_p)$ and 100 eV $(3.35U_p)$ are sketched in Fig. 1(c). For one recollision energy smaller than the maximum one, the trajectory with an earlier ionization time and a later recombination time is called a long trajectory, while the one with a later ionization time and an earlier recombination time is called a short trajectory. The classical trajectories can be divided into three sections, taking

the cutoff trajectory as an example: i) the electron is 'Accelerated Away' from the parent ion after ionized at time t_1 [the point A in Fig. 1(a)], and moves in the continuum till the time when the field becomes zero [the point B in Fig. 1(a)]; ii) the electron is 'Decelerated Away' to the excursion

$$S^{\rm ex} = S(t_3) = \int_{t_1}^{t_3} \left(\int_{t_1}^{t'} \mathcal{E}_1(t'')\,{\rm d}t'' \right) {\rm d}t', \tag{15}$$

where t_3 [denoted as the point C in Fig. 1(a)] is the time when the velocity is zero, satisfying the equation

$$\int_{t_1}^{t_3} \mathcal{E}_1(t)\,{\rm d}t = 0; \tag{16}$$

iii) the electron is 'Accelerated Back' to the parent ion till the time t_2 when the recombination happens [the point D in Fig. 1(a)] and the kinetic energy obtained in the interval from t_3 to t_2 plus the potential energy is converted into the harmonic radiation.

In Fig. 1(d), the five trajectories related to the recollision energies denoted in Fig. 1(c) are plotted in the velocity–position plane. One can see that the electron starts from the nucleus located at the position (0) with zero velocity, and returns to its parent ion at the position (0) through different trajectories which depend on the ionization time and the electric field during the propagation. The intersection of the trajectory with the velocity axis represents the recollision velocity or the recollision kinetic energy when the recombination may happen, and the intersection with the position axis represents the maximum distance from the nucleus which the electron can reach, i.e., excursion $S^{\rm ex}$ of the trajectory. The trajectories can be recognized with its excursion $S_{\rm ex}$ in the velocity–position plane: the cutoff trajectory with $S^{\rm ex}_{\rm cutoff} = -85.3$ a.u. forms the division between the short and long trajectories. The short trajectories with shorter propagation time correspond to $|S^{\rm ex}| < |S^{\rm ex}_{\rm cutoff}|$, while the long trajectories with longer propagation time correspond to $|S^{\rm ex}| > |S^{\rm ex}_{\rm cutoff}|$. For a given recollision energy, the derivative ${\rm d}v/{\rm d}x$ of the long trajectory becomes negative before the recombination happens but the derivative ${\rm d}v/{\rm d}x$ of the short trajectory holds positive during the whole 'Accelerated Back' process. It means that the electron following the long trajectory suffers from the deceleration of the field before recolliding with its parent ion but the acceleration process for the electron following the short trajectory has not ended when the recombination happens. In contrast, the cutoff trajectory with the highest recollision energy has a proper large excursion so that the electron is accelerated in the whole period from t_3 to t_2 to make the electron recollision energy

$$E_k = \frac{1}{2}\left(\int_{t_3}^{t_2} \mathcal{E}_1(t)\,{\rm d}t \right)^2, \tag{17}$$

be maximal.

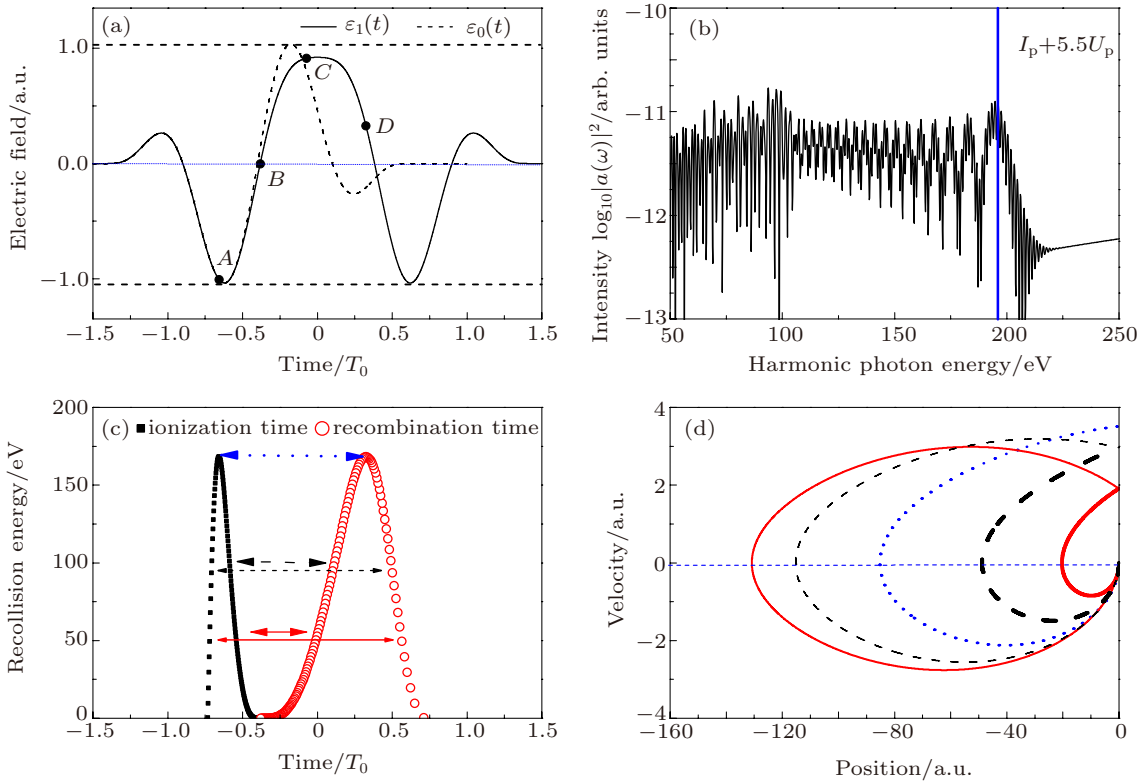


Fig. 1. (color online) (a) The electric fields of $\mathcal{E}_1(t)$ (solid line) and $\mathcal{E}_0(t)$ (dotted line). $I = 5 \times 10^{14}$ W·cm^{-2}, $\omega = 0.057$ a.u. (a.u. is the abbreviation for atomic unit), and $\tau = 0.8T_0$. (b) The harmonic spectrum from He atom generated by $\mathcal{E}_1(t)$. (c) The dependence of the recollision energy on the ionization time (black solid squares) and recombination time (red open squares) in $\mathcal{E}_1(t)$. (d) The velocity–position plot of the five trajectories sketched in Fig. 1(c), the cutoff trajectory (blue dotted line), the short (red thick solid line) and long (red thin solid line) trajectories with $E_k = 1.67U_{\rm p}$, and the short (black thick dashed line) and long (black thin dashed line) trajectories with $E_k = 3.35U_{\rm p}$. The direction of trajectories are clockwise.

Equation (17) indicates that the electron recollision energy at the end of electron trajectories is determined by the waveform of the laser field in the final (Acceleration Back) section. Here we note that, besides the waveform in the integral, one should also pay an attention to the lower limit of the integral in Eq.(17), t_3, which is the starting time of the Acceleration Back section. In the velocity–position plane, t_3 is characterized by $S^{\rm ex}$. Equations (15) and (16) suggest that $S^{\rm ex}$ is determined by the waveform in the previous two sections of the trajectory. Thus the waveform in all three sections of the electron trajectory, not only the Acceleration Back section, should be optimized to achieve enhancement of the electron recollision energy. Generally speaking, besides synthesizing the waveform in the final (Acceleration Back) section, one should also optimally shape the waveform in the Acceleration Away and Deceleration Away sections to make the cutoff trajectory have an optimized $S^{\rm ex}_{\rm cutoff}$, which maximizes the 'absorption' of field energy and transfers all the 'absorbed' energy to the emitted photon without loss in the field.

4. Enhancement of electron recollision energy via optimal-shaped waveform

Based on the analysis in the previous section, we will optimize the waveform of a laser field by two steps in this section. In the first step, we synthesize the laser field $\mathcal{E}_2$ [plotted in Fig. 2(a)] by adding a flat-top in the field $\mathcal{E}_1$ to modify the Acceleration Back process. The resulting field $\mathcal{E}_2$ has the waveform

$$\mathcal{E}_2(t) = \begin{cases} \mathcal{E}_1(t), & \text{if} \quad t < 0, \\ \mathcal{E}_1(t-P), & \text{if} \quad t > P, \\ \mathcal{E}_1(0), & \text{if} \quad 0 \le t \le P, \end{cases} \tag{18}$$

where $P = 0.162T_0$ is the length of the flat-top. Figure 2(b) is the HHG spectrum generated from $\mathcal{E}_2$. It is shown that the cutoff frequency is extended up to $I_{\rm p}+8.98U_{\rm p}$. In the velocity–position plane (Fig. 3), the trajectories are plotted simultaneously for the two laser fields $\mathcal{E}_1(t)$ and $\mathcal{E}_2(t)$ to investigate the effect of the added flat-top on the Acceleration Back section. For the trajectories in the different laser fields but with the equal $S^{\rm ex}$, such as the long trajectory of $E_k = 3.35U_{\rm p}$ in $\mathcal{E}_1(t)$ and the short trajectory of $E_k = 8.81U_{\rm p}$ in $\mathcal{E}_2(t)$, their excursions are the same ($S^{\rm ex} = -120.5$ a.u.), and thus the increased recollision energy must be attributed to the synthesized flat-top. It can be understood as follows: the synthesized flat-top modifies the Acceleration Back section of the long trajectory with $S^{\rm ex} = -120.5$ a.u., making the electron be accelerated in the whole period from t_2 to t_3. Therefore, the long trajectory in $\mathcal{E}_1(t)$ becomes the short one in $\mathcal{E}_2(t)$. The same change is made to all the trajectories with -132.7 a.u.$< S^{\rm ex} < -85.3$ a.u. As a result, the cutoff trajectory $S^{\rm ex}_{\rm cutoff}$ is moved from -85.3 a.u. to -132.7 a.u., the maximum recollision energy $E_{\rm max}$ is raised from $5.5U_{\rm p}$ to $8.98U_{\rm p}$ correspondingly.

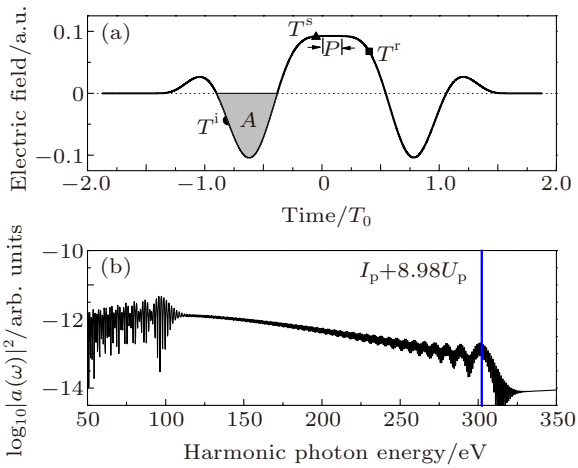


Fig. 2. (color online) (a) The electric fields of $\mathcal{E}_2(t)$. The parameters are the same as those in Fig. 1(a) except $P = 0.162T_0$. (b) The harmonic spectrum from the He atom generated by $\mathcal{E}_2(t)$.

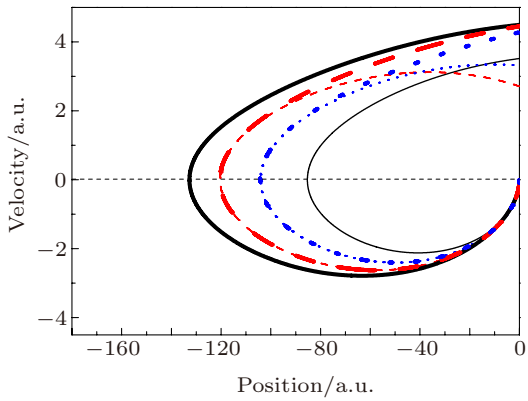


Fig. 3. (color online) Comparison of the electron trajectories in the velocity–position plane. For the trajectories in $\mathcal{E}_1(t)$, the cutoff trajectory with $E_k = 5.5U_{\rm p}$ is shown with a black thin solid line, the long trajectory with $E_k = 4.91U_{\rm p}$ is shown with a blue thin dotted line, and the long trajectory with $E_k = 3.35U_{\rm p}$ is shown with a red thin dashed line. For the trajectories in $\mathcal{E}_2(t)$, the cutoff trajectory with $E_k = 8.98U_{\rm p}$ is shown with a black thick solid line, the short trajectory with $E_k = 8.81U_{\rm p}$ is shown with a red thick dashed line, and the short trajectory with $E_k = 8.13U_{\rm p}$ is shown with a blue thick dotted line. The direction of trajectories are clockwise.

The ionization time $T^{\rm i}$ (solid cycle), recombination time $T^{\rm r}$ (solid rectangle), and the time $T^{\rm s}$ (solid uptriangle) at the moment reaching the excursion of the cutoff trajectory in $\mathcal{E}_2(t)$ are sketched in Fig. 2(a). Maintaining the slope $\mathrm{d}v/\mathrm{d}x(>0)$ as large as possible in the whole Acceleration Back section of the cutoff trajectory, the field with the flat-top structure accelerates the electron back to its parent ion with a higher recollision energy. It is also noted that the highest recollision energy obtained by synthesizing a flat-top structure is limited by the largest $S^{\rm ex}$ the electron can reach, which is finally determined by the longest Acceleration Away section the trajectory can have [the gray area in Fig. 2(a) marked by A]. Thus in the second step, an optimal-shaped waveform $\mathcal{E}_3(t)$ [shown in

Fig. 4(a)] is proposed,

$$\mathcal{E}_3(t) = \mathcal{E}_0(t + 3\tau/2)\,\mathrm{e}^{\mathrm{i}\pi} + \mathcal{E}_2(t), \tag{19}$$

to extend the excursion. In $\mathcal{E}_3(t)$, as marked in Fig. 4(a), a long flat-top P is added to make the electron be accelerated as long as possible and raise the recollision energy, and in contrast to the field $\mathcal{E}_2(t)$ a flat-bottom profile 'f' is synthesized to generate a large S^{ex} with effective ionization rates. Figure 4(b) shows the harmonic spectrum generated by $\mathcal{E}_3(t)$. Three plateaus are observed in the harmonic spectrum, whose cutoff frequencies are about $I_\mathrm{p} + 5.5U_\mathrm{p}$, $I_\mathrm{p} + 20.26U_\mathrm{p}$, and $I_\mathrm{p} + 18.85U_\mathrm{p}$, respectively.

To relate certain trajectories with the three cutoff frequencies, the dependences of the recollision energies on the ionization and recombination times are presented in Fig. 4(c). It is shown that there are two major return events contributing to the harmonic generation within the first return of the electron. In the first event R_1, the ionization and recombination happen at $T_1^{\mathrm{i}} = -1.45T_0$ and $T_1^{\mathrm{r}} = -0.47T_0$, respectively and the maximum recollision energy $E_{\max}^1$ is $5.5U_\mathrm{p}$. It is generated from the waveform [the part before the N point in Fig. 4(a)], which is the same as the main part of $\mathcal{E}_1(t)$ except the reversed sign. In the second event R_2, the ionization and recombination happen at $T_2^{\mathrm{i}} = -0.91T_0$ and $T_2^{\mathrm{r}} = 0.81T_0$, respectively, and the maximum recollision energy $E_{\max}^2$ is $20.26U_\mathrm{p}$. It is generated from the waveform after the M point in Fig. 4(a). In Fig. 4(c), we also represent the dependence of the recollision energy on the ionization and recombination times for the electron's second return to its parent ion. In the major event in the second return R_3, the ionization and recombination happen at $T_3^{\mathrm{i}} = -1.38T_0$ and $T_3^{\mathrm{r}} = 0.83T_0$, respectively, and the maximum recollision energy $E_{\max}^3$ is $18.85U_\mathrm{p}$. The trajectories corresponding to $E_{\max}^1$, $E_{\max}^2$, and $E_{\max}^3$ are plotted with the black dotted, blue solid, and red dashed lines, respectively, in the velocity–position plane [Fig. 4(d)]. One can see that the excursion S^{ex} of the trajectories corresponding to $E_{\max}^2$ and $E_{\max}^3$ are increased as high as -276.7 a.u. and -265.5 a.u. due to the synthesized flat-bottom profile. And the trajectories, accelerated by the flat-top structure, lead to the recollision energies as high as $20.26U_\mathrm{p}$ and $18.85U_\mathrm{p}$. We note that these two maximum recollision energies are much higher than that presented in Ref. [14]. It is because in Ref. [14], the duration of electron trajectory was fixed when synthesizing the ideal waveform but in our study the durations of cutoff trajectories are enlarged due to the increased excursion S^{ex} in $\mathcal{E}_3(t)$.

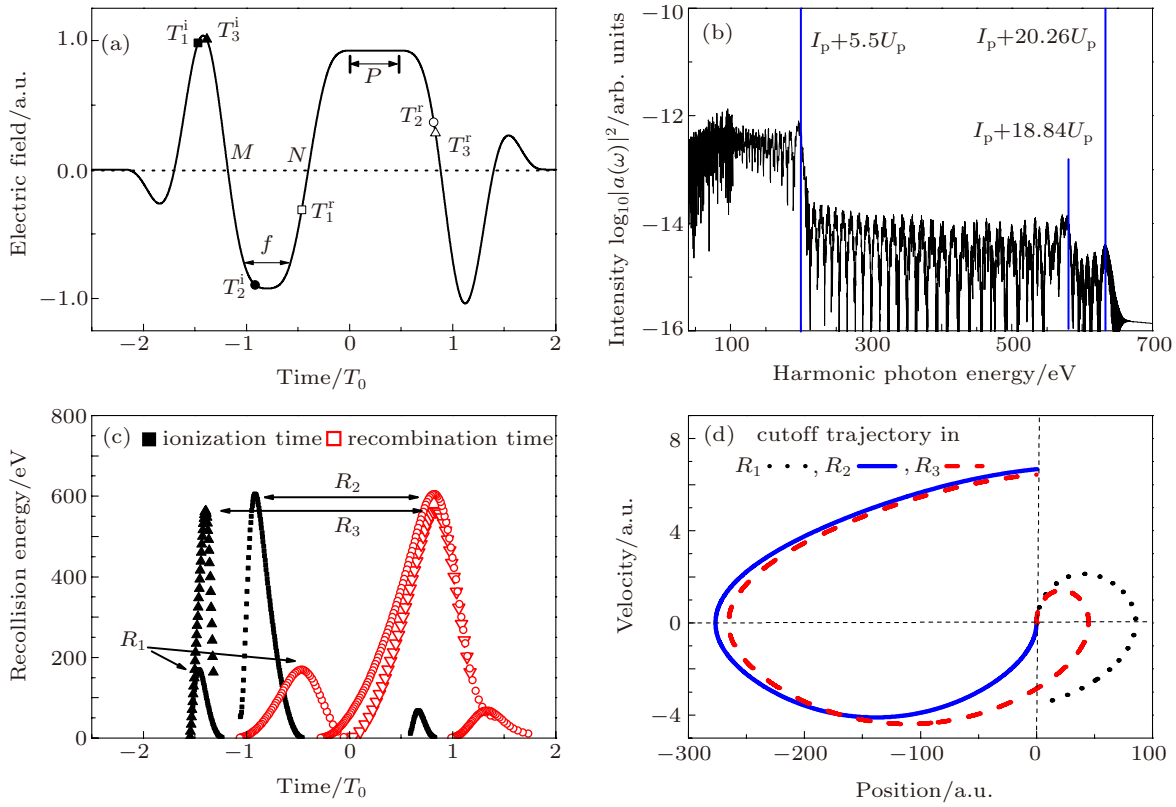


Fig. 4. (color online) (a) The electric field of $\mathcal{E}_3(t)$, the parameters are the same as those in Fig. 3(a) except $P = 0.5T_0$. The ionization times (T_1^{i}, T_2^{i}, and T_3^{i}) of the three cutoff trajectories are labeled by solid rectangle, cycle, and uptriangle points, respectively. The recombination times (T_1^{r}, T_2^{r}, and T_3^{r}) of the three cutoff trajectories are labeled by hollow rectangle, cycle, and uptriangle points, respectively. (b) The harmonic spectrum from the He atom generated by $\mathcal{E}_3(t)$. (c) The dependence of recollision energy on the ionization (black solid squares for the first return and black solid uptriangles for the second return) and recombination times (red open cycles for the first return and red open downtriangles for the second return) in $\mathcal{E}_3(t)$. The three major return events, R_1, R_2, and R_3, are sketched. (d) The velocity–position plot of the trajectories corresponding to the three cutoff frequencies generated by $\mathcal{E}_3(t)$. The direction of trajectories is clockwise.

In Fig. 4(b), the amplitudes of the two plateaus with the cutoff frequencies $I_p + 20.26U_p$ and $I_p + 18.85U_p$ are smaller than that of the plateau with the cutoff frequency $I_p + 5.5U_p$. The decrease of the harmonic amplitude is due to the extra electron wave packet spreading, i.e., the direct result of the increase of the duration of trajectories. However, it is also noted that the major return event R_3 has a larger amplitude in the spectrum than the event R_2 does, although the duration of electron trajectories in R_3 is longer than those in R_2. It means that the spreading of an electron wave packet may be reduced by the 'focusing' effect of the parent ion when the electron wave packet goes through the ion region. This provides a potential approach to overcome the reduction of the harmonic amplitude that is caused by the spreading of electron wave packets.

5. Conclusion

In this paper, the HHG spectra in strong laser fields are investigated by employing the strong-field approximation. Within the strong-field approximation, the classical electron trajectories of the ionized electron moving in the continuum are analyzed in the velocity–position plane. It is shown that the electron recollision energy depends on not only the waveform in the 'Accelerated Back' section of the classical electron trajectory, but also the excursion amplitude determined by the waveform in the 'Accelerated Away' and 'Decelerated away' sections. Therefore, to achieve the highest recollision energy, one needs to optimally design the waveform of the laser fields by considering all the three sections simultaneously. We propose a synthesized waveform of the laser field which has a flat-bottom in the 'Accelerated Away' and 'Decelerated away' sections, and a flat-top in the 'Accelerated Back' section, respectively. We find that the cutoff frequency can be extended up to $I_p + 20.26U_p$ by the use of the designed waveform. The three cutoff frequencies in the harmonic spectrum are explained by the analysis of the classical electron trajectory quite well.

References

[1] Gibson E A, Paul A, Wagner N, Tobey R, Gaudiosi D, Backus S, Christov I P, Aquila A, Gullikson E M, Attwood D T, Murnane M M and Kapteyn H C 2003 *Science* **302** 95

[2] Seres E, Seres J, Krausz F and Spielmann C 2004 *Phys. Rev. Lett.* **92** 163002

[3] Takahashi E J, Kanai T, Ishikawa K L, Nabekawa Y and Midorikawa K 2008 *Phys. Rev. Lett.* **101** 253901

[4] L'Huillier A and Balcou P 1993 *Phys. Rev. Lett.* **70** 774

[5] Ravasio A, Gauthier D and Maia F R N C 2009 *Phys. Rev. Lett.* **103** 028104

[6] Winterfeldt C, Spielmann C and Gerber G 2008 *Rev. Mod. Phys.* **80** 117

[7] Kapteyn H C, Murnane M M and Christov I P 2005 *Phys. Today* **58** 39

[8] Corkum P B 1993 *Phys. Rev. Lett.* **71** 1994

[9] Zhang X, Lytle A L, Popmintchev T, Zhou X, Kapteyn H C, Murnane M M and Cohen O 2007 *Nat. Phys.* **3** 270

[10] Zepf M, Dromey B, Landreman M, Foster P and Hooker S M 2007 *Phys. Rev. Lett.* **99** 143901

[11] Steingrube D S, Vockerodt T, Schulz E, Morgner U and Kovačev M 2009 *Phys. Rev. A* **80** 043819

[12] Tate J, Auguste T, Muller H G, Sali'eres P, Agostini P and Dimauro L F 2007 *Phys. Rev. Lett.* **98** 013901

[13] Colosimo P, Doumy G, Blaga C I, Wheeler J, Hauri C, Catoire F, Tate J, Chirla R, March A M, Paulus G G, Muller H G, Agostini P and Dimauro L F 2008 *Nat. Phys.* **4** 386

[14] Chipperfield L E, Robinson J S, Tisch J W G and Marangos J P 2009 *Phys. Rev. Lett.* **102** 063003

[15] Pfeifer T, Gallmann L, Abel M J, Nagel P M, Neumark D M and Leone S R 2006 *Phys. Rev. Lett.* **97** 163901

[16] Hong W, Lu P, Lan P, Yang Z, Li Y and Liao Q 2008 *Phys. Rev. A* **77** 033410

[17] Zhang G T, Wu J, Xia C L and Liu X S 2009 *Phys. Rev.* A **80** 055404

[18] Song X, Zeng Z, Fu Y, Cai B, Li R, Cheng Y and Xu Z 2007 *Phys. Rev. A* **76** 043830

[19] Wu J, Zhang G T, Xia C L and Liu X S 2010 *Phys. Rev. A* **82** 013411

[20] Zeng Z, Cheng Y, Song X, Li R and Xu Z 2007 *Phys. Rev. Lett.* **98** 203901

[21] Zhai Z and Liu X S 2008 *J. Phys. B: At. Mol. Opt. Phys.* **41** 125602

[22] Lan P, Lu P, Cao W, Li Y and Wang X 2007 *Phys. Rev. A* **76** 011402

[23] Faria C F, Dörr M, Becker W and Sandner W 1999 *Phys. Rev. A* **60** 1377

[24] Li X X, Xu Z Z and Mao L Q 1997 *Acta Phys. Sin.* (Overseas Edition, i.e. *Chin. Phys.*) **6** 197

[25] Ye X L, Zhou X X, Zhao S F and Li P C 2009 *Acta Phys. Sin.* **58** 1579 (in Chinese)

[26] Xiang Y, Niu Y and Gong S 2009 *Phys. Rev. A* **79** 053419

[27] Carrera J J and Chu S I 2007 *Phys. Rev. A* **75** 033807

[28] Xu J, Zeng B and Yu Y 2010 *Phys. Rev. A* **82** 053822

[29] Xiao J, Sun Z R, Wang Y F, Deng L, Zhang X Y, Chen G L, Zhang W P, Wang Z G, Xu Z Z and Li R X 2005 *Chin. Phys. Lett.* **22** 873

[30] Bao M Q and Starace A F 1996 *Phys. Rev.* A **53** R3723

[31] Milošević D B and Starace A F 1999 *Phys. Rev. Lett.* **82** 2653

[32] Milošević D B and Starace A F 1999 *Phys. Rev. A* **60** 3160

[33] Odžak S and Milošević D B 2005 *Phys. Rev. A* **72** 033407

[34] Wang B B, Li X F and Fu P M 1995 *Chin. Phys. Lett.* **15** 195

[35] Hong W, Lu P, Cao W, Lan P and Wang X 2007 *J. Phys. B: At. Mol. Opt. Phys.* **40** 2321

[36] Moreno P, Plaja L and Roso L 1997 *Phys. Rev. A* **55** R1593

[37] Numico R, Moreno P, Plaja L and Roso L 1998 *J. Opt. Soc. Am. B* **31** 4163

[38] Bandrauk A D, Barmaki S and Kamta G L 2007 *Phys. Rev. Lett.* **98** 013001

[39] Lewenstein M, Balcou Ph, Ivanov M Y, L'Huillier A and Corkum P B 1994 *Phys. Rev. A* **49** 2117

[40] Lai X Y, Cai Q Y and Zhan M S 2009 *New J. Phys.* **11** 113035

[41] Pérez-Hernández J A, Hoffmann D J, Zaïr A, Chipperfield L E, Plaja L, Ruiz C, Marangos J P and Roso L 2009 *J. Phys. B: At. Mol. Opt. Phys.* **42** 134004

[42] Milošević D B 2006 *J. Opt. Soc. Am. B* **23** 308